Supplementary Information for
Switching of Perpendicular Nanomagnets with Spin Orbit Torque without an External Magnetic Field by Engineering a Tilted Anisotropy

Long You[1], OukJae Lee[1], Debanjan Bhowmik[1], Dominic Labanowski[1], Jeongmin Hong[1], Jeffrey Bokor[1], Sayeef Salahuddin[1,2]

[1] Department of Electrical Engineering and Computer Sciences, University of California at Berkeley, Berkeley, California 94720, USA,

[2] Materials Sciences Division, Lawrence Berkeley National Laboratory, Berkeley, California 94720, USA

SI Text

S.1 *M-H* Charactersitic of thin films

The magnetic properties of Ta (10 nm)/CoFeB (1 nm)/MgO (1 nm)/Ta(~ 3nm) thin films, which were used for device fabrication in this work, were measured by using a Vibrating Sample Magnetometer (VSM). Figure S1 shows the normalized in-plane and out-of-plane magnetization versus external magnetic field (*M-H*) curves. The *M-H* loops indicate that the film possesses a perpendicular easy axis with anisotropy field, H_K, around 5K Oe, and out-of-plane coercivity, H_c, around 30 Oe.

S.2 Micromagnetic simulation of magnetization state of nanomagnet with a single wedge:

Nanomagnet with one side wedge is simulated using micromagnetics. The geometry of structure is shown in Fig. S3. The width of nanomagnet is 90 nm. The total length of the nanomagnet is 300 nm. The length of wedge part in –x direction (K2 = 0) is 60 nm. This part has zero perpendicular anisotropy since there is no interface anisotropy caused by the MgO/CoFeB interface. The interface anisotropy K1 of non-wedge part is assumed to be 6 x 105 J/m3. Mesh size across the thickness is ~3 nm or in other words. 4 layers are simulated in OOMMF on top of each other at 0.3 nm separation with decreasing length from bottom to top to simulate the wedge.

Starting from the magnetization in +z direction with an intentionally slight tilt in +y direction, the system is allowed to evolve. The magnetization then evolves in a few nanoseconds to the final state from initial +z shown in the Fig. S4 for four different layer. The arrows here signify the moments in the wedge region are tilted towards +x, so the net moment is tilted towards +x. Note that the magnetization equilibrium state is finally tilted towards +x direction, it does not matter what the intentionally slight tilt direction is, such as –y, +x, -x (we did not show here).

On the contrary, starting from the magnetization in -z direction with a intentionally slight tilt in +y, the magnetization evolves in a few nanoseconds to the final state shown in the Fig. S5. The arrows here signify the moments in the wedge region are tilted towards –x. We observe that the magnetization goes to final state in tilting to –x, in four initially slight tilting (+y, -y, +x, -x) cases.

Therefore, the tilt of the axis is either in +x or –x direction based on the slope of the wedge. In our case, the wedge is on the -x and the magnet is longer at the bottom and shorter at the top. The anisotropy axis as a result tilts along the surface of the wedge. This minimizes the magnetostatic energy of the system. As a result when $m_z \sim 1$ (the magnetization in z direction), it will be tilted to the +x direction and when $m_z \sim -1$ (the magnetization in z direction), it will be tilted to the -x direction.

S.2.1: Magnet starting from x-axis:

Next, we simulate the final magnetic state of nanomagnet with similar wedge (in –x direction) as our experiment, when the magnetization initially start from +x and –x direction. The magnet with wedge on the left is simulated by considering a magnet of dimensions 300 nm by 90 nm by 1.2 nm with a mesh size of 0.3 nm across the thickness (z direction). The wedge is simulated by making the length of the bottom layer 300 nm and gradually narrowing the length of the layers such that the top layer is 240 nm. Starting from the moments in the +x direction, the final state of the magnet is shown as Fig. S6. We see in the final state the moments are predominantly in +z direction with a small reverse domain. Such reverse domain is formed due to minimize the dipole

coupling of the system. Similarly, starting from the magnetic moments in the –x direction, the final state of the magnet is in –z direction (we do not show here).

This initial condition is of particular interest because it can be created by spin orbit torque from current pulse where current flows along the y-axis, as we have done in our experiments. The micromagnetic simulations shown in this section shows that once the magnet is placed in along the x-axis and current is taken of, then depending on whether it started from +x or –x, it will go to +z or –z direction as we have seen in our experiments.

S.2.2. Dependence of the tilt angle on the shape of the wedge

The tilting angle depends upon the ratio of the length of the wedge to the length of the magnet. In the figure S7, we show through simulation that the tilting angle changes based on the length of the wedge to the magnet. The thickness of the ferromagnet changes from 1 nm to 0 along the wedge. We start from the magnetization in the out of plane direction (+z) and let the system relax. The final in-plane component of the magnetization, which is in the +x direction due to the shape of the wedge, is proportional to the tilt angle. We show that higher the ratio of the length of the wedge to the length of the magnet, greater is the x-component of the final magnetization, and hence greater is the tilt angle.

S.3. AMR measurement

In general, the dependence of the anisotropic magnetoresistivity on the angle φ between the spontaneous magnetization M_S and the current flow direction I in the geometry of Fig. S9 a and b can be written by

$$\rho(\varphi) = \rho_{\perp} + (\rho_{//} - \rho_{\perp})\cos^2\varphi = \rho_{\perp} + \Delta\rho\cos^2\varphi \qquad \text{(S1)}$$

where $\rho_{\perp}$ ($\rho_{//}$) is the resistivity when M is saturated perpendicular (parallel) to the I. The change in θ, the angle between in plane field H_{inp} and I, leads to a variation in φ that leads to an oscillatory behavior between the maximum value and minimum value. However, if the anisotropy axis is slightly tilted from $\hat{z}$ axis, the projection of $\hat{M}$ onto xy plane is not collinear with H_{inp}. The angle between H_{inp} and the projection of $\hat{M}$ onto xy plane, is denoted as η. This

angle is defined to be positive, when it rotates from H_{inp} to the projection of $\hat{M}$ onto xy plane in a counter-clockwise direction. Otherwise, the angle η is negative. Therefore, based on our definition and the coordinates used in our sample geometry, the AMR varied with the angle θ can be written in the following form if we ignore constant value $\rho_{\perp}$:

$$\rho(\theta) = \Delta\rho\cos^2\varphi = \Delta\rho\cos^2\gamma(\cos\theta - \sin\theta\tan\eta)^2 \qquad \text{(S2)}$$

where γ is the angle between $\hat{M}$ and H_{inp} and $\gamma < 90^{\circ}$. From the equation S2, the minimum resistivity ρ_{min} is found at θ=90°-η ($\cos\theta = \sin\theta\tan\eta$) instead of θ=90° ($\cos\theta = 0$), if the anisotropy axis tilted away from $\hat{z}$. Specifically, if the anisotropy axis tilts towards $+\hat{x}$, η is positive (η >0), as shown in Fig. S9. This causes the ρ_{min} to appear at θ=90°-η<90°, which is found in the AMR measurement when we applied in-plane field of 1000 Oe in our nanomagnet initially saturated upward . On the contrary, if the anisotropy axis is tilted towards $-\hat{x}$, the angle η <0. This causes the ρ_{min} arises at θ=90°-η>90°, which is found in the AMR measurement when we applied in-plane field of 1000 Oe in our nanomagnet initially saturated in downward (blue dots in Fig. 3b; the minimum resistivity appears when θ is around 100°). Furthermore, the AMR is also asymmetric with respect to the x-axis. If the anisotropy axis tilted towards $+\hat{x}$, when H_{inp} is rotated away from x-axis, the γ decreases monotonically, causing $\cos^2\gamma$ to increase monotonically, which leads to $\rho(0^{\circ}) < \rho(180^{\circ})$. This asymmetry is observed in our measurement by applying 1000 Oe in-plane field when nanomagnet is initially saturated upward, specifically, $\rho(0^{\circ}) \cong 0.7\rho(180^{\circ})$. In contrast, $\rho(0^{\circ}) > \rho(180^{\circ})$ is expected when the anisotropy axis tilted towards $-\hat{x}$, which is found in the nanomagnet initially saturated downward, driven by 1000 Oe in-plane field.

In order to clearly understand the variation of AMR with θ, numerical modeling of AMR as a function of θ is required. Here a single domain model is used for AMR simulation assuming uniaxial anisotropy field (H_K) is 3500 Oe. With the coordinates as shown in Fig. S8, the relevant magnetic energy per unit volume (E) can be expressed as the sum of Zeeman (E_Z) and uniaxial anisotropy (E_a) energies:

$$E = E_z + E_{an} = -H_{IP}M_s\cos\gamma(\theta) + K_u\sin^2\beta(\theta) \qquad \text{(S3)}$$

Where β is the angle between the anisotropy axis and $\hat{M}$, M_s the saturation magnetization. K_u is the uniaxial anisotropy constant, which is equal to $H_K \bullet M_s/2$. We numerically obtain the θ angle which minimizes E and then calculate the AMR (for each value of H with a fixed θ orientation). The numerical simulation results (black lines) match the experiments (symbols) well, if we assume anisotropy axis tilting 2° from $+\hat{z}$ towards $+\hat{x}$ or from $-\hat{z}$ towards $-\hat{x}$. Moreover, AMR curves show an almost $\cos^2\theta$ dependence regardless of the initial magnetization direction when the in-plane field is as high as 3000 Oe, which is due to the fact that the contribution of last term in equation S(2), $\sin\theta\tan\eta$, to AMR is now negligible.

S.4. Comparison of the Anomalous Hall effect exhibited by nanomagnets of different shapes

In order to see the magnetic properties of nanomagnet without a wedge and in-plane shape anisotropy, a circularly shape nanomagnet (diameter D= 200 nm) without a wedge was nanofabricated using the same process and stack as the rectangularly shaped nanomagnet which we used in this paper. The anomalous Hall effect (AHE) for a circular shaped nanomagnet was measured and compared with that of the nanomagnet as shown in Fig. S10. The AHE loop for the circular nanomagnet exhibits a strong perpendicular magnetic anisotropy (PMA) and a remanent magnetization that points completely out of plane. In other words, the remnance ratio (the ratio between anomalous Hall effect resistance at zero field R_{rem} and saturation field R_{sat}) is equal to 1, as shown in Fig. S10. In comparison, the perpendicular component of magnetization for the patterned rectangular magnet with wedge shows increasing AHE resistance with increase of external field up to the coercive field.

S.5. Comparison of Tilt angles:

As shown in section S3, using *a tilt angle of 2˚*, we obtain very good fitting of the experimental data Importantly, AMR measurement also provides the direction of the tilt angle, as mentioned in the main text. Note, however, that there is an uncertainty of 1˚ in the direction of magnetic field.

It is also possible to estimate the tilt angle from the slant of the R-H loop (from AHE) in the saturation region by using

$$\theta_m = \cos^{-1}\left(\frac{m_{rem}}{m_{rem,ref}}\right) = \cos^{-1}\left(\frac{M_{rem}/M_{sat}}{M_{rem,ref}/M_{sat,ref}}\right) = \cos^{-1}\left(\frac{R_{rem}/R_{sat}}{R_{rem,ref}/R_{sat,ref}}\right) \quad (1)$$

where m_{rem} is the normalized remanance (M_{rem}/M_{sat}) and $m_{rem,ref}$ is the reference remanance of a strong PMA magnet. This method gives the tilt angle to be roughly 5°.
Thus the two methods show that the tilt angle is between 2-5˚.

S.6. Current induced switching of the magnet:

S.6.1. R-I loop:

Fig. S11 (a) and (b) show the R_{AHE}-H and R_{AHE}-I loops respectively. Note that for the R_{AHE}-I loop, the remnant state of the magnet after applying a current pulse is plotted. When a large DC current is flowing, there could be significant resistance drift and therefore R_{AHE} measured during the current flow is noisy and unreliable. This is why the remnant state is measured for the R_{AHE}-I loop.

S.6.2. Histogram of the switching possibility P_{sw} when the current is flowing along the long axis of the nanomagnet

Figure S12 shows the switching results of all trials for the four devices shown in the main text, when the same switching current densities were applied along the long axis. For four devices, both the upward to downward and downward to upward switching occurs, by either positive (along $+\hat{x}$) or negative (along $-\hat{x}$) critical current pulses. It is interesting to note that two 100% switching possibilities occur, one is upward to downward switching on device #3 by positive critical current pulse, and other is downward to upward switching on device #1 by negative critical current pulse. However, a high switching possibility (60%) occurs when critical current pulse polarity is changed and applied on these two devices. This indicates no deterministic switching occurs on any device.

S.7.In-plane current switching of a square nanomagnet

We investigate switching behavior of a square nanomagnet by injecting the current pulse along one side, without an external magnetic field. This device was fabricated from the same stack as used in the main text, Ta (10 nm)/CoFeB (1 nm)/MgO (1 nm)/Ta (~ 10 nm capping layer). Scanning electron microscopy (SEM) images of a square nanomagnet (200 nm × 200 nm) at the centre of a symmetric Hall bar, as shown in Fig. S13a. We measure the anomalous Hall effect resistance R_H. Measurements clearly show that the easy axis of the square nanomagnet is in the out-of-plane direction, as shown in Fig. S13b. Next, starting from an up position a current pulse of magnitude 1.5×10^7 A cm^{-2} and of 1 s duration was applied 30 times. The possibility p_{sw} of finial state going "up" and "down" states are around 0.57 and 0.43, respectively (Fig. S13c). The near 50% probability of 'up' and 'down' states show that it is not possible to switch the magnet deterministically without an external field.

S.8. Analysis of current induced longitudinal and transverse effective field

The current-induced effective field is measured in CoFeB layers based on the combination of the of the 1st and 2nd harmonic contributions of the anomalous Hall effect (AHE). Here, we estimate the effective field induced by current flowing into 20μm×20μm Hall bar comprised of same stack as the nanomagnets. The in-phase first harmonic (V_ω) and the out-of-phase second harmonic ($V_{2\omega}$) signals are measured simultaneously, when we apply a constant amplitude a.c voltage to the Hall bar, as shown in Fig. S14. When we sweep the in-plane field oriented transverse (H_T, along ±y) or parallel (H_L, along ±x) to the current flow, the transverse (ΔH_T) and longitudinal (ΔH_L) effective fields are obtained by using the following equations [S1]:

$$\Delta H_{T(L)} = -2 \frac{\dfrac{\partial V_{2\varpi}}{\partial H_{T(L)}}}{\dfrac{\partial^2 V_{\varpi}}{\partial H^2{}_{T(L)}}} \qquad \text{(S4)}$$

Using equation (S4), we calculation ΔH_T and ΔH_L for the input voltage V_{IN} (11.3 mV) , which corresponds to a current density of $\sim 1.34 \times 10^6$ Acm^{-2} if we assume uniform current flow across the Ta layer and the CoFeB layer. ΔH_T and ΔH_L are estimated for both magnetization states (pointing along +Z and –Z). We find that ΔH_T (Rashba field) is independent of the magnetization

direction and is around 25.3 Oe, whereas the sign reverses for ΔH_L (effective field produced by spin Hall effect), the magnitude is around 5.8 Oe, and the spin Hall angle is estimated to be around 0.09.

S.9. Simulations of temperature increase:

We have performed a COMSOL simulation to calculate the temperature rise (see Fig. S15). After injecting 1.25 mA current, the highest temperature rise calculated is around 20 K. This shows that temperature rise is not of critical importance in our experiments.

Room temperature is set to 293.15 K in the simulation. A convective heat flux of 5 W/(m^2K) is applied on the top surface of the sample, and the bottom surface of the substrate is kept at room temperature. Substrate thickness is set to be 400 um. Temperature of the device is plotted after application of 1.25 mA between the left and right terminals for 1 second.

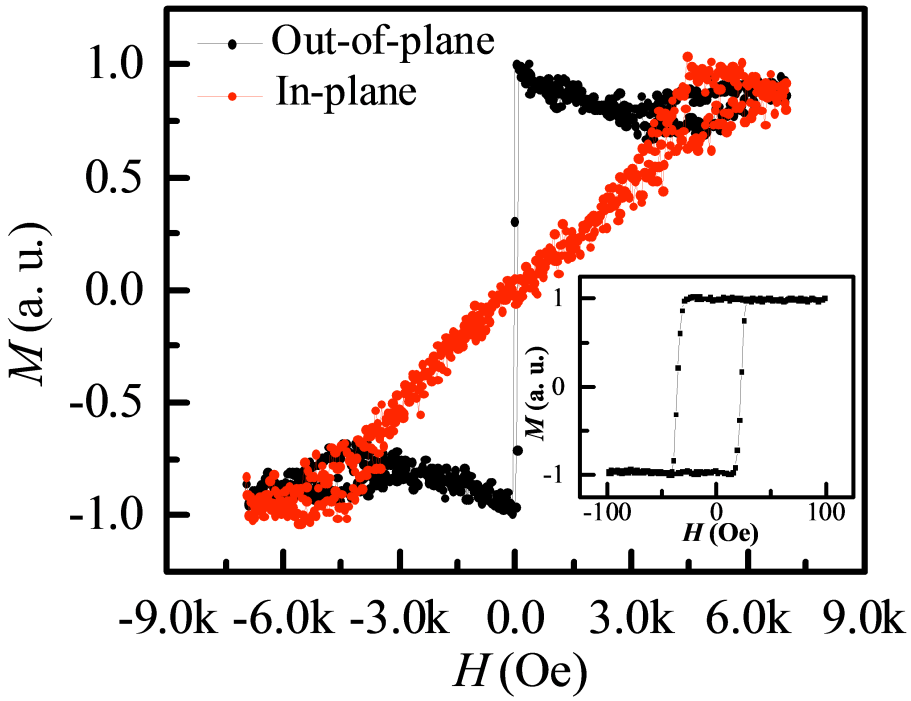

Figure S1: In-plane and out-of-plane magnetic loops of Ta (10 nm)/CoFeB (1 nm)/MgO (1 nm)/Ta(~3 nm) (from substrate). Inset: the out-of-plane *M*-*H* loop was measured at low magnetic field.

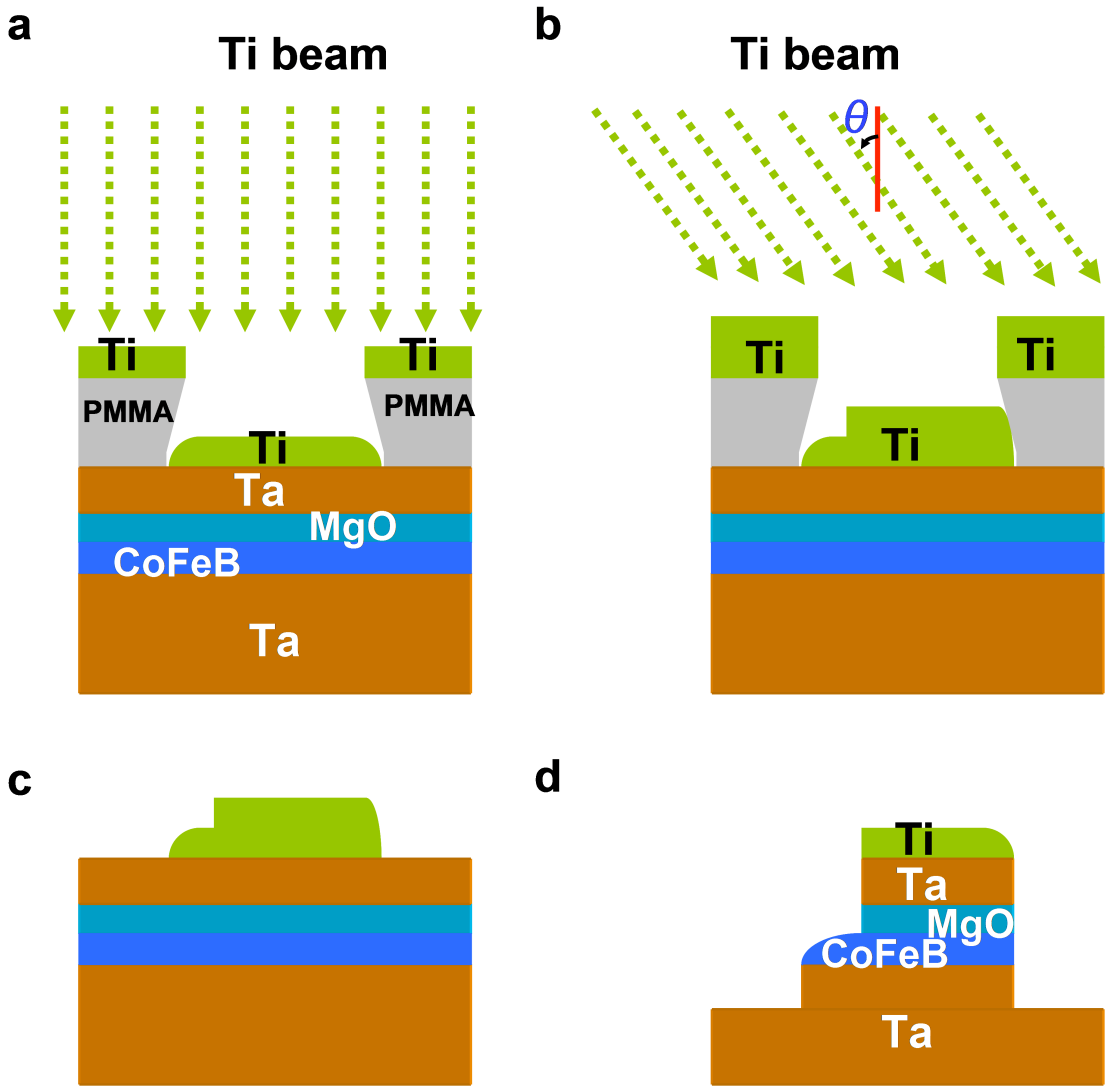

Figure S2 Illustrations of electron beam lithography and a wedge shape creation. a, Schematic diagram of the patterned resist for the normal deposition of the sample; b, Schematic diagram of the oblique deposition of the sample; c, Schematic diagram of the deposition of the patterned hard mask metal Ti with stack; d, Schematic diagram of the final nanomagnet with a wedge shape on one side of device.

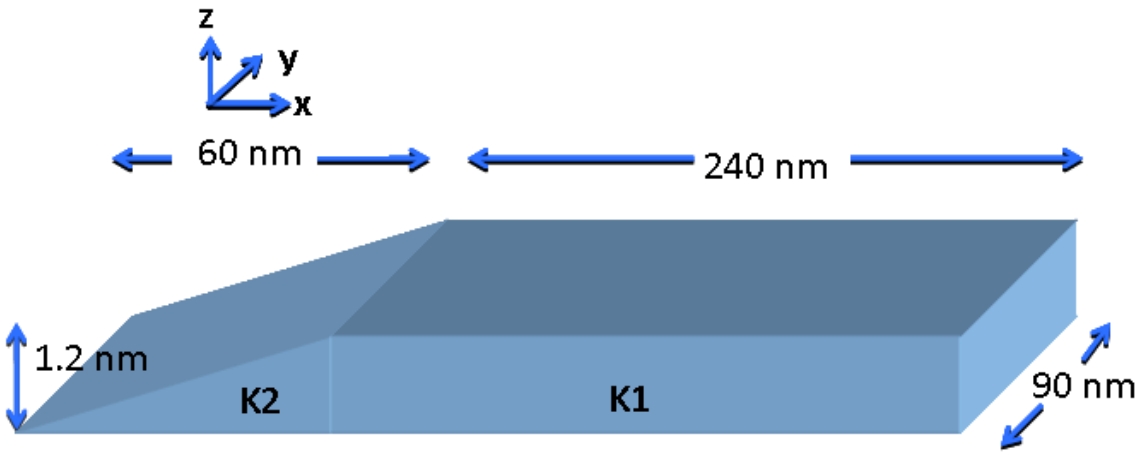

Fig.S3 Schematic configuration of nanomagnet with one side wedge in –x direction for micromagnetic simulation. The width of nanomagnet is 90 nm. The total length of the nanomagnet is 300 nm. The length of wedge part with zero interface anisotropy ($K_2 = 0$) is 60 nm. The interface anisotropy K_1 of non-wedge part is 6 x 10^5 J/m^3.

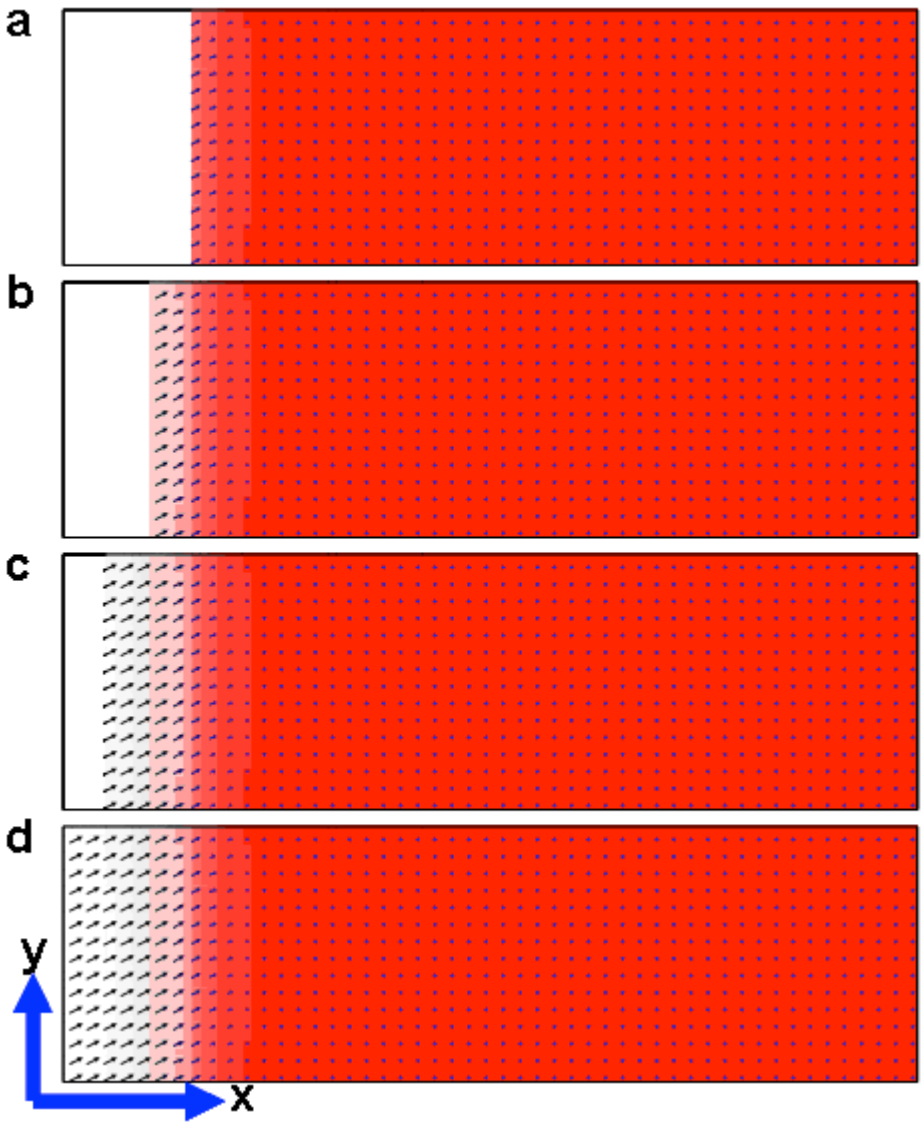

Figure S4 Final magnetic state of the nanomagnet with one wedge in -x for initial state of magnet in +z direction with slight tilt in +y direction for (a) uppermost layer, (b) second layer, (c) third layer and (d) lowest layer. Blue dot in red color implies the magnet is out of plane (+z). The arrows here signify the moments in the wedge region are tilted towards +x; so the net moment is tilted towards +x.

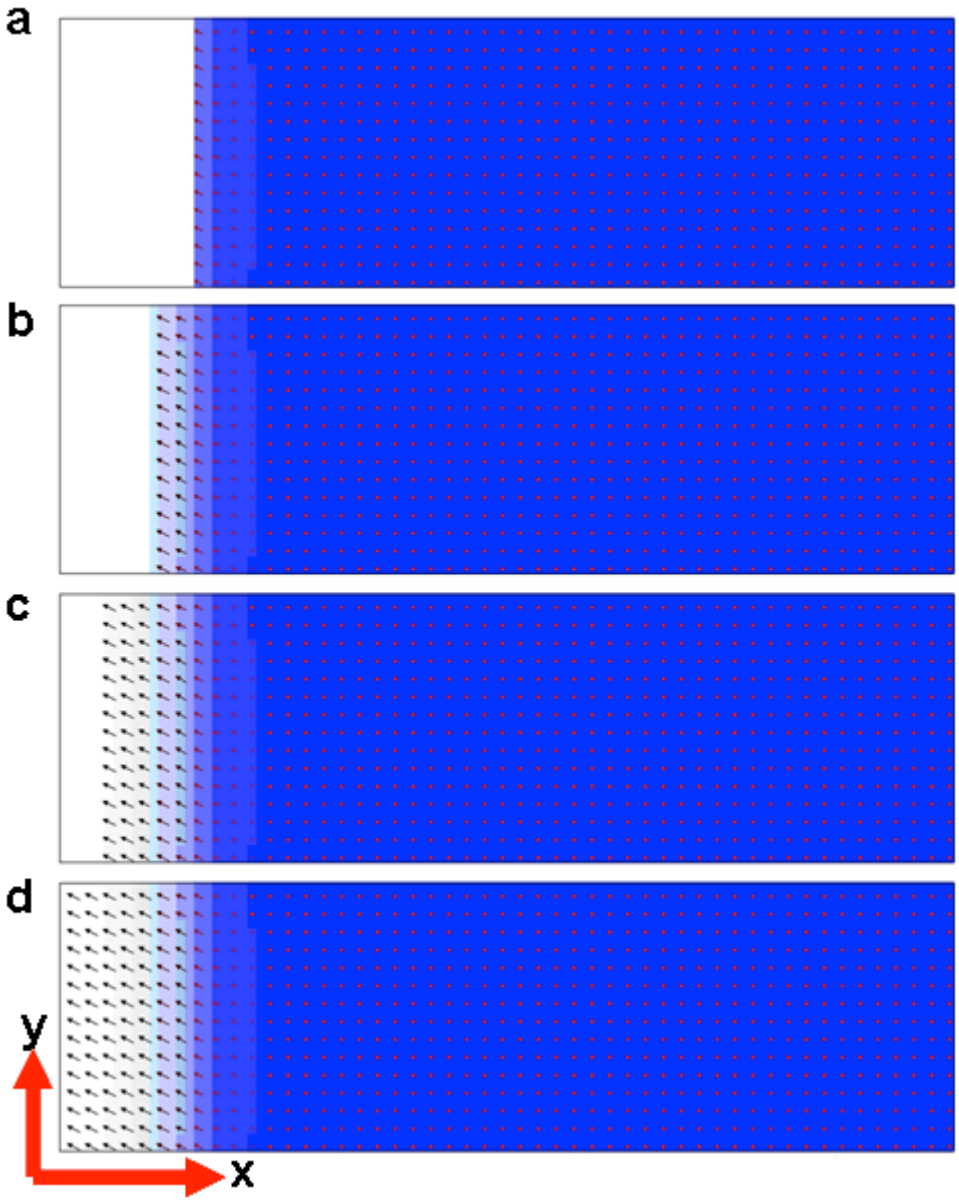

Figure S5 Final magnetic state of the nanomagnet with one wedge in -x for initial state of magnet in -z direction with slight tilt in +y direction for (a) uppermost layer, (b) second layer, (c) third layer and (d) lowest layer. Red dot in blue background color implies magnet is into the plane (-z). The arrows here signify the moments in the wedge region are tilted towards -x; so the net moment is tilted towards -x.

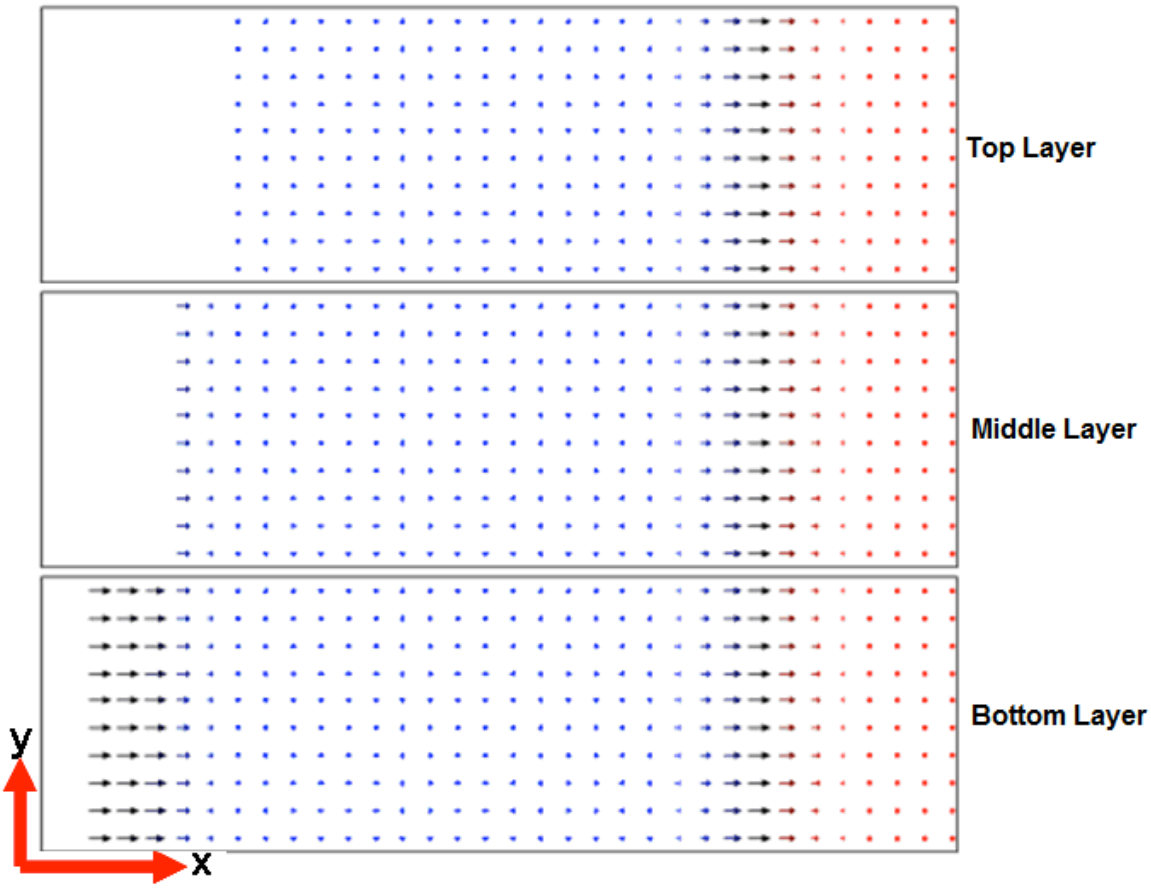

Figure S6 Final magnetic state of the nanomagnet with one wedge in -x starting from the moments in the +x direction for top layer, middle layer and bottom layer. Blue dots mean moments are out of the plane (+z) direction while red dots mean moments are into the plane (-z) direction.

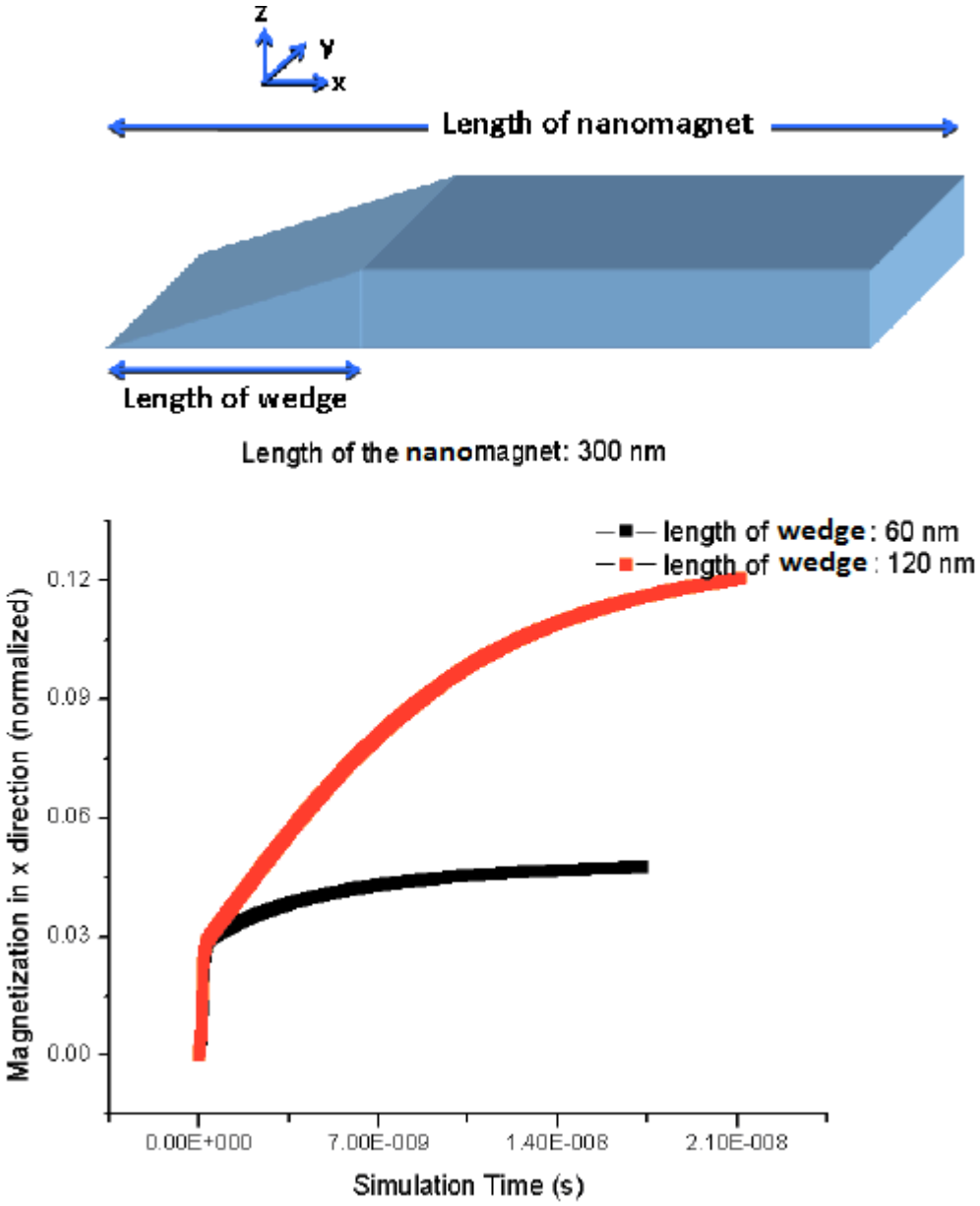

Figure S7 The time evolution of the magnetization component m_x of a nanomagnet with a wedge length of 60 nm or 120 nm in –x direction. The total length of nanomagnet is 300 nm. As we can see from the figure above, when the length of the wedge is 60 nm, tilt angle= $\sin^{-1}$ (0.045)= 2.58° while when the length of the wedge is 120 nm, tilt angle= $\sin^{-1}$(0.12)=6.89°.

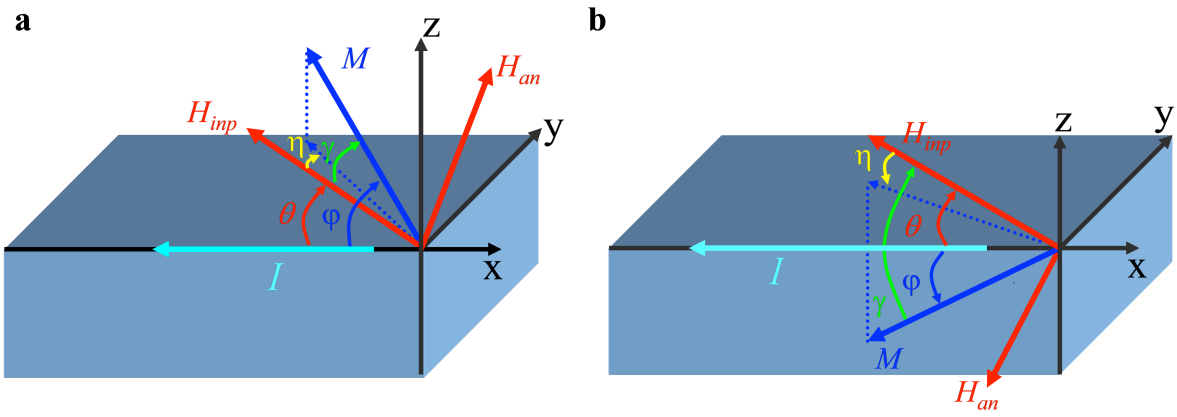

Figure S8: Schematic representation of the coordinate system used in our AMR measurements assuming anisotropy axis tilted (a) from $\hat{z}$ to $\hat{x}$ and (b) from $-\hat{z}$ to $-\hat{x}$. The sense current I flows along $-\hat{x}$ direction oriented long axis of nanomagnet. $\theta = 0$ corresponds to the orientation where the applied field is aligned to the current ($-\hat{x}$), the direction of θ was taken as positive for a clockwise rotation of the field from current. γ is the angle between external in-plane field H_{inp} and φ is the angle between M and I. The angle η is measured from the H_{inp} to the projection of $\hat{M}$ onto $\hat{x}\hat{y}$ plane; the angle is defined to be positive when it rotates in a counter-clockwise direction.

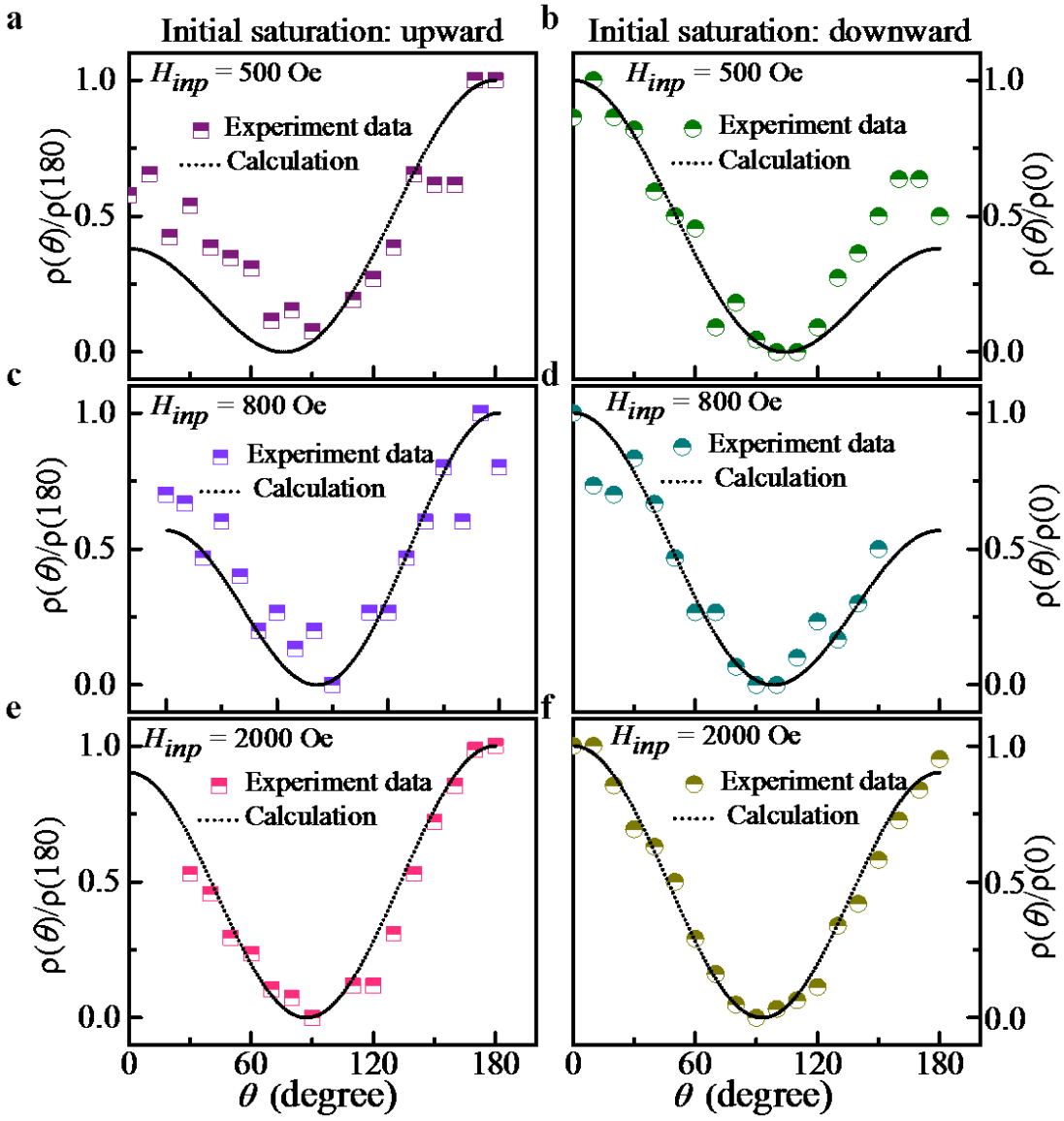

Figure S9: The angular dependence of the anisotropic magnetoresistance (AMR) of a rectangular nanomagnet when current flows along along -x direction pointing to the long axis of the nanomagnet. AMR curves were measured as a function of the angle θ between current and in-plane magnetic field, and were compared with simulated results using a single-domain model with sensor current flowing along long axis of nanomagnet. Calculated and measured values of AMR resistivity are shown when $|H_{inp}|$=500 Oe and the magnet was initially polarized (a) upward and (b) downward. Calculated and measured values of AMR resistivity are shown when $|H_{inp}|$=800 Oe and the magnet was initially polarized (c) upward and (d) downward. Calculated and measured values of AMR resistivity are shown when $|H_{inp}|$=2000 Oe and the magnet was initially polarized (c) upward and (d) downward.

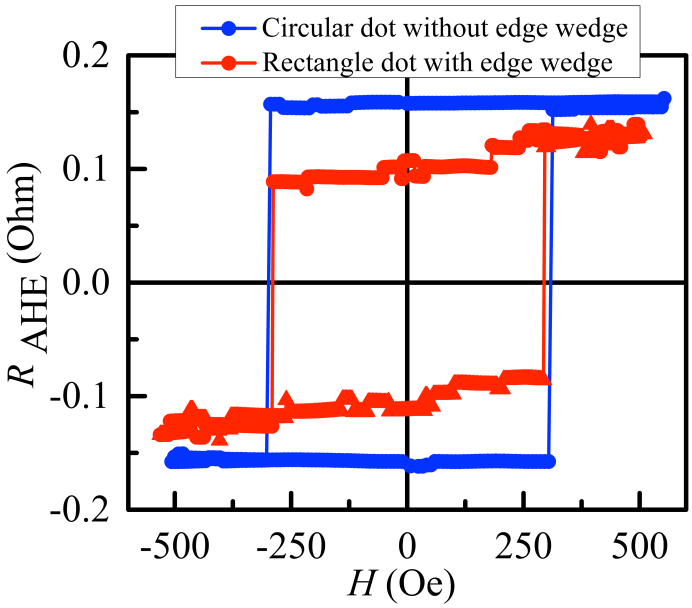

Figure S10: Dependence of anomalous Hall effect resistance with applied field for both rectangular shaped nanomagnet with a wedge at one side along long axis and circular-shaped nanomagnet without a wedge.

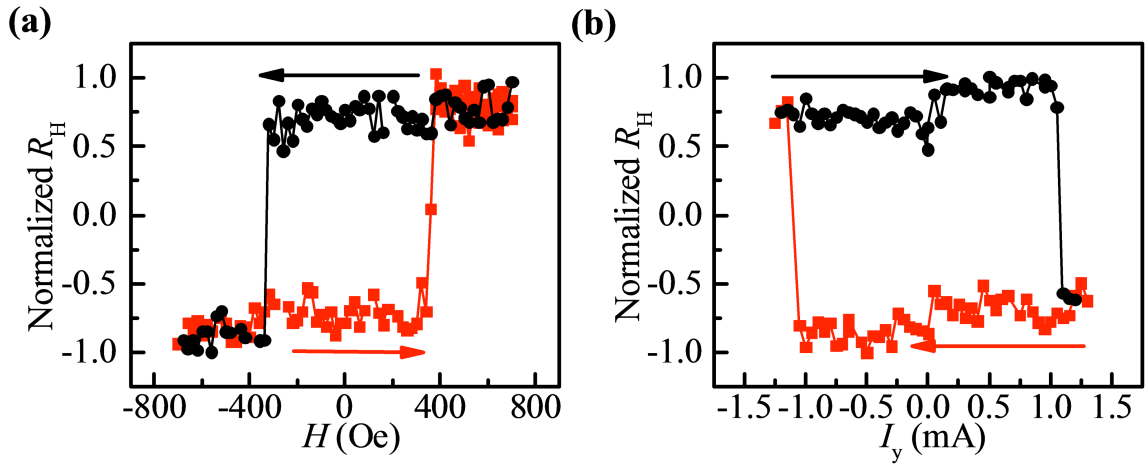

Figure S11 Spin Hall effect–induced switching for a nanomagnet with tilting anisotropy a, M_z measured by the anomalous Hall resistance as a function of applied field, b. M_z measured after the injection of positive (black circles) and negative (red squares) current pulses with 1 s pulse duration.

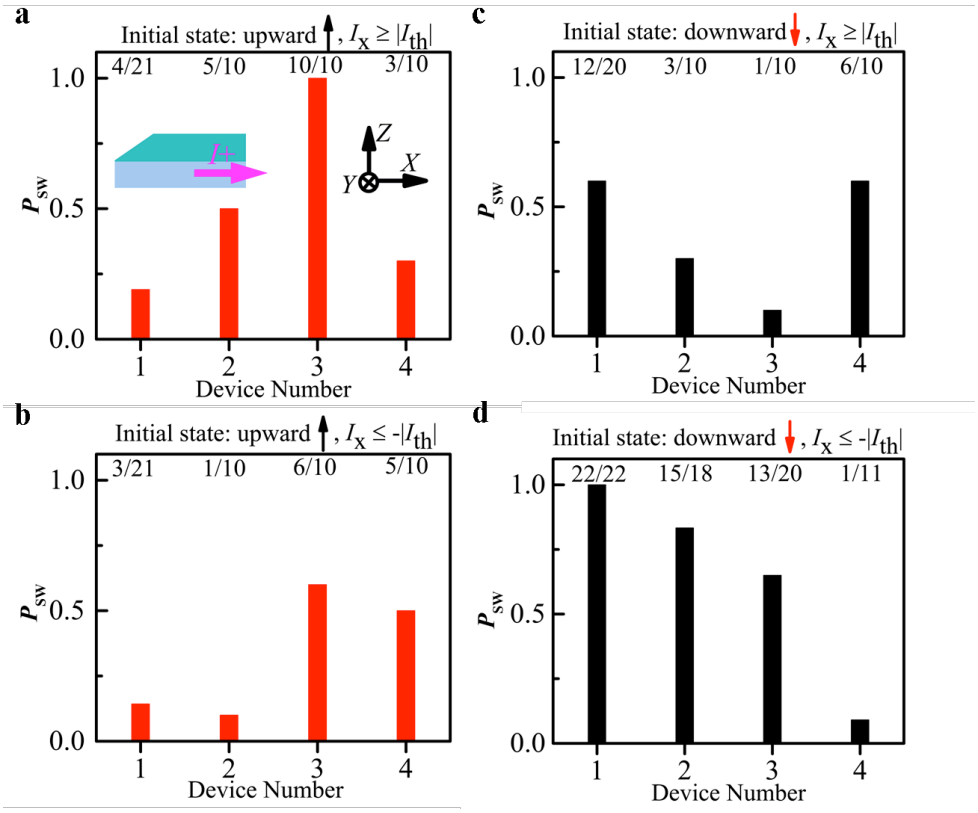

Figure S12: Histogram of the switching possibility P_{sw} on four devices by injecting in-plane current along long axis of nanomagnet. The upward to downward switching possibility (a) by current pulse along $+\hat{x}$, (b) by negative current pulse along $-\hat{x}$, and the downward to upward switching possibility (c) by positive current pulse along $+\hat{x}$, (d) by negative current pulse along $-\hat{x}$.

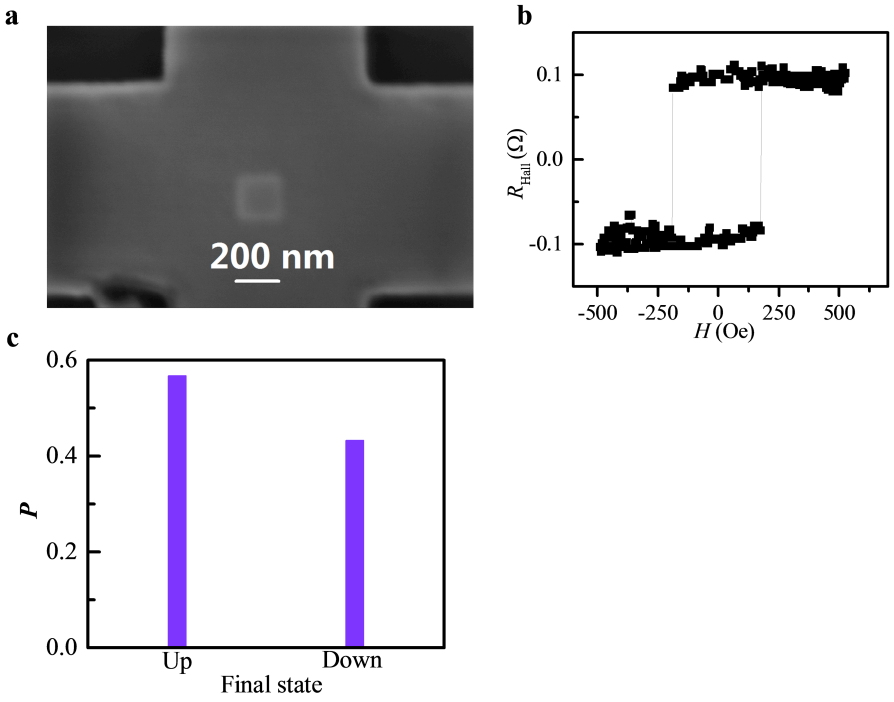

Figure S13: In plane current induced switching of square nanomagnet. (a) SEM image of a square nanomagnet (side length ~200 nm) on top of Ta, which forms a symmetric Hall bar structure for current injection and AHE detection. The device is fabricated from the stack of Ta (10 nm)/CoFeB (1 nm)/MgO (1 nm)/Ta (~10 nm, capping layer), (b) The anomalous Hall resistance R_H as a function of magnetic field H when H is applied along the easy axis (perpendicular to the film plane), (c) Histogram of switching probability p_{sw} after application of a current pulse of magnitude 1.5×10^7 A cm^{-2} in the absence of an external magnetic field.

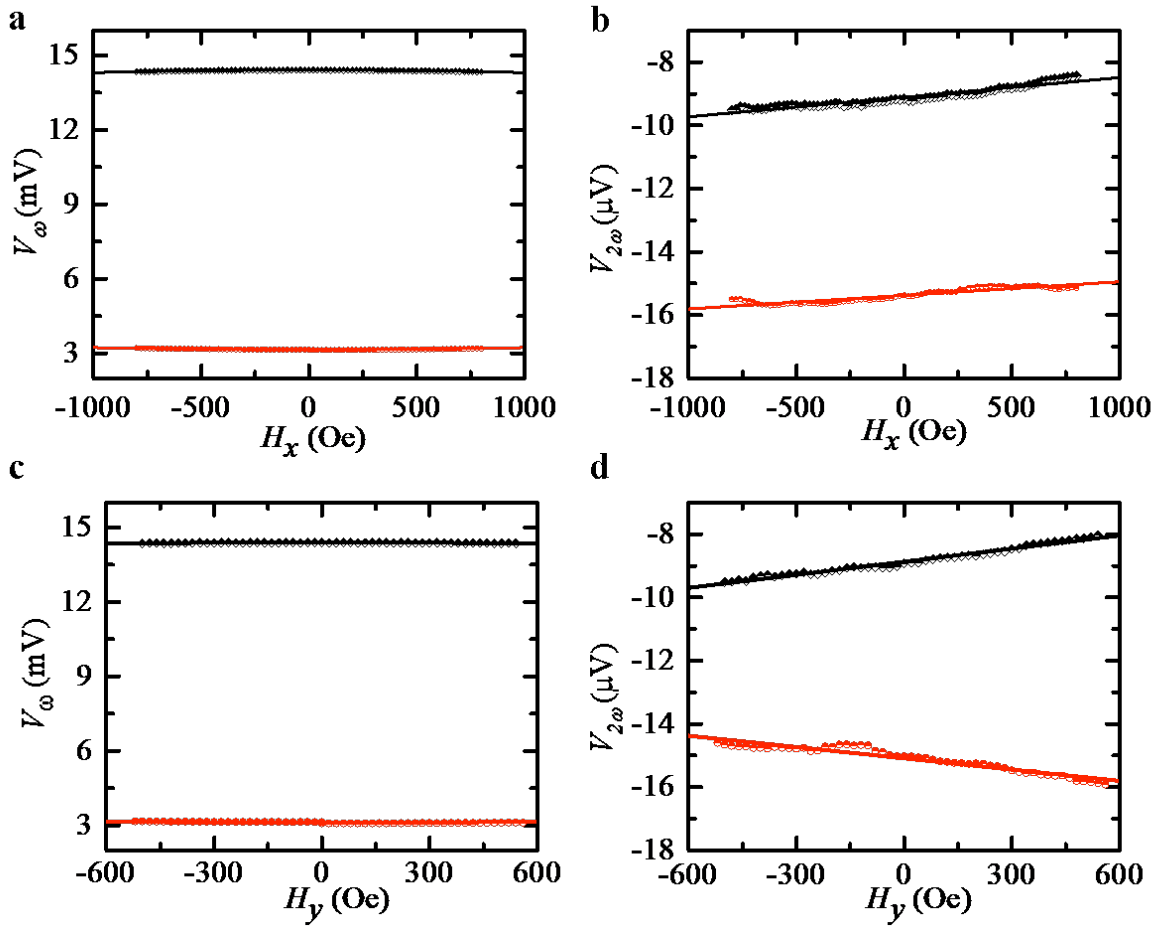

Figure S14. First and second-harmonic signals illustrating current induced effective field in a 20 μm × 20 μm Hall bar comprised of Ta (10 nm)/CoFeB (1 nm)/MgO (1 nm)/Ta (capping layer) stack, same as that for our nanomagnet. (a,c) The in-phase first harmonic (V_ω) signals and (b, d) 90° out of phase second-harmonic signal $V_{2\omega}$ are plotted as a function of an in-plane field, which is (a, b) parallel and (c,d) transverse to the current flow. The black and red symbols represent the magnetization of the samples (along + Z and − Z, respectively).

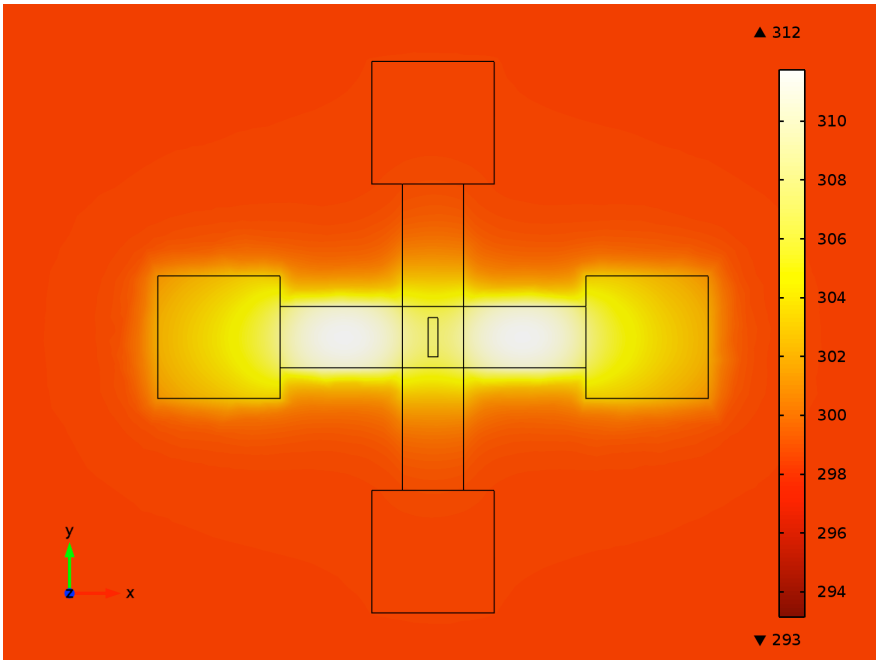

Figure S15: Simulated temperature as a function of x-y position on the top surface of a device.

Supplementary References

[S1] Kim, J., *et al.* (2013) Layer thickness dependence of the current-induced effective field vector in Ta/CoFeB/MgO. *Nature Mater.* 12: 240-245.

[S2] Donahue, M. J. and Porter, D. G. (1999) OOMMF User's Guide, Ver. 1.0, Interagency Report NISTIR 6376, NIST, USA.

[S3] You, C. Y. (2012) Micromagnetic Simulations for Spin Transfer Torque in Magnetic Multilayers, J. Magn. 17: 73-77.

[S4] Liu, L. Q. *et al*. (2012) Spin-torque switching with the giant spin Hall effect of tantalum. *Science* 336: 555–558.